Inelastic Scattering Dynamics of Hyperthermal Fluorine Atoms on a Fluorinated Silicon Surface

Timothy K. Minton*

Department of Chemistry and Biochemistry, Montana State University, Bozeman, Montana 59717

Konstantinos P. Giapis* and Teresa Moore

Division of Chemistry and Chemical Engineering, California Institute of Technology, Pasadena, California 91125

Received: February 28, 1997; In Final Form: May 16, 1997[⊗]

The interaction of energetic fluorine atoms with a fluorinated silicon surface has been studied by monitoring energy and angular distributions of scattered fluorine atoms. Two beams with average translational energies of 284 and 544 kJ/mol were directed onto the SiF_x layer, known to exist during steady-state etching. While thermal scattering of unreacted fluorine atoms is observed, nonthermal scattering dominates and includes both single- and multiple-bounce collisions at the complex surface. Multiple-bounce collisions often lead to a near-thermal (cosine) distribution of exit angles but incomplete thermalization of translational energy. A hard-sphere kinematic model, based on single atom−surface collisions, can be used to predict the overall average energy transfer as a function of deflection angle, indicating that the complex scattering events at the surface can appear *on average* like single collisions.

I. Introduction

Gas−surface interaction dynamics are of central importance in many physical and chemical processes.[1] The interaction of energetic ions with semiconductor surfaces, in particular, determines the outcome of plasma etching, the technique of choice for submicron pattern transfer in microelectronics.[2] The inelastic and reactive scattering dynamics of such interactions influence etch rates and the shape of sidewalls, both of which are vitally important for efficient fabrication of integrated circuits.[3,4] Plasma etching has evolved thus far mostly by an empirical approach (process development), while a basic understanding of the underlying chemical physics has lagged behind.[5] However, as device dimensions shrink to meet demands for semiconductor chips with faster processing speeds and denser memories, profile irregularities can no longer be tolerated. Their origin must be understood before judicious solutions can be offered.[2,4] The complexity of the plasma environment requires that the elementary phenomena be examined in well-characterized beam experiments so that meaningful conclusions can be deduced. Then, the combination of fundamental scattering experiments with numerical simulations of the etching process can lead to deeper understanding and improved processing.[2−5]

Modern high-density plasma reactors typically operate at low (<20 mTorr) pressures and produce ions with translational energies in the 5−50 eV range.[6] In this relatively low-energy regime, however, the possibility that unreacted etchant species will scatter and react on subsequent collisions at evolving sidewalls can no longer be overlooked. For example, inelastic scattering of unreacted fluorine ions on a fluorinated silicon surface at the bottom of a trench may result in a significant flux of energetic fluorine atoms at the sidewalls, where etching could cause material removal under the mask (undercutting). The scattering dynamics must be understood in order to develop etch models that will enable better process control and mitigation of effects that lead to undesirable etching characteristics.[4,7] The scattering dynamics are inextricably linked with etch profile evolution and may be revealed by experimental measurements of the angular flux and velocity distributions of the scattered atoms. However, these measurements need to be performed under realistic etching conditions if connections with processing technology are desired. The semiconductor surface must be in a similar state in terms of species and coverage (e.g., a thick fluorinated silicon layer exists during etching of silicon with fluorine-based chemistry). Therefore, fluxes of reactive species must be adequate to achieve reasonable etch rates and maintain steady state. Although frequently used, beams of reactive ions may cause surface charging, especially when semiinsulating substrates are used, thus deflecting low-energy ions and making angularly resolved measurements difficult. No significant charging of unpatterned surfaces occurs in plasmas because the surface layer is simultaneously bombarded with electrons which neutralize the charge. To prevent charging effects on experimental measurements, neutral atomic beams are preferable. We have described a hyperthermal fluorine-atom beam source which we have used in preliminary studies of etching and reactive scattering on a silicon surface.[8] The scattering dynamics with neutral atoms are not expected to differ from those occurring when plasma ions impinge on a surface because most ions undergo Auger neutralization before striking the surface and may then interact as neutral atoms. In addition, fast neutrals, produced by charge exchange collisions, may exist in high-density plasmas, rendering experiments with neutral beams even more relevant.

The collisions that mediate energy transfer and scattering direction when an energetic fluorine atom strikes a silicon surface during etching are likely to be governed by surface corrugation. During etching of silicon with fluorine-based chemistry, a complex fluorinated layer is formed, consisting of SiF_3, SiF_2-SiF_3, and $SiF_2-SiF_2-SiF_3$ moieties which protrude from the surface.[9] On this rough surface, multiple-bounce interactions could be important, if not dominant. At the high atom−surface collision energies that would be useful in etching,

* Authors to whom correspondence should be addressed.
[⊗] Abstract published in *Advance ACS Abstracts,* July 15, 1997.

S1089-5639(97)00767-6 CCC: $14.00

multiple-bounce interactions might become especially important because surface penetration will enhance the effective surface roughness. Furthermore, at high incident energies, more collisions on the surface will be required to achieve thermal equilibrium. Thus, the hyperthermal regime of collision energy raises the distinct possibility of an important multiple-bounce interaction where incident atoms lose a significant fraction of their incident energies but scatter away before reaching thermal equilibrium with the surface. If enough bounces occur, memory of the incident angle could be lost and the angular distribution of scattered atoms might appear thermal even while the energy distribution is still hyperthermal. Indeed, successful modeling of experimental silicon etch profiles required the assumption of significant scattering of fluorine atoms with slightly hyperthermal energy distributions but thermal angular distributions.[3] Also, unresolved structure in the translational energy distributions of energetic argon atoms scattering from liquid metals[10] and from liquid perfluorinated polyether[11] indicated an incompletely thermalized component that suggests multiple bounce inelastic scattering.

Considering the importance of scattering dynamics in modern etching environments and the probable intricacies of the dynamics under the unique conditions of collision energy and surface complexity, we undertook a detailed study of hyperthermal fluorine atom scattering dynamics on a silicon surface. The experiments were conducted in a molecular beam apparatus that allowed energy and angular resolution of the scattered atoms. Preliminary results of the scattering dynamics were reported with a model of etch profile evolution.[3] Here we present a thorough description of the dynamics and demonstrate the importance of multiple-bounce scattering and the limited utility of a hard-sphere kinematic model to describe energy transfer at the atom−surface interface.

II. Experimental Details

The hyperthermal beam source and molecular beam apparatus have been described earlier.[8] Laser detonation of SF_6 gas in the confined region of a conical nozzle was used to produce pulses (at 1.8 Hz) of energetic atomic fluorine and sulfur with a nominal direction. Atomization is typically greater than 96%, and the ion fraction in the beam is estimated to be $<<1\%$. The central portion of the beam exited the source chamber through a 3 mm diameter skimmer ~80 cm from the apex of the conical nozzle. The beam was further collimated with a second 1.8 mm diameter aperture 2 cm downstream from the skimmer. At 92 cm from the nozzle apex, the beam pulse, having approximately the diameter of the second aperture, impinged on a target surface, whose rotation axis was coincident with the rotation axis of a mass spectrometer detector. The estimated F-atom flux at the target position is 2×10^{14} atoms/cm^2/s. The distance from the target surface to the detector ionizer was 34.5 cm. With the use of the detector, time-of-flight (TOF) distributions of inelastically scattered atoms were collected in the plane of the beam axis and surface normal as a function of incident (θ_i) and exit (θ_f) angles (with respect to the surface normal). The detector geometry and beam spot size on the surface yielded a total angular viewing range of $\leq 2°$. A chopper wheel, placed 85 cm from the nozzle apex, was used to select a narrowed velocity distribution from the overall beam pulse. The chopper had the additional benefit of blocking all light emitted by the source plasma and essentially all the residual ions, which travel at higher velocities than most of the atoms in the neutral beam pulse.

The beam was interrogated with the mass spectrometer detector by positioning the detection axis along the beam axis and lowering the target out of the beam path. Figure 1 shows the translational energy distribution of the overall F-atom beam pulse and the narrowed distributions which describe the two beams used in these experiments. The average incident energies E_i were 284 and 544 kJ/mol with energy widths (full width at half-maximum) of 49 and 124 kJ/mol, respectively. The areas of the distributions in Figure 1 are proportional to flux; therefore, the F-atom flux ratio between the higher- and lower-energy beams was 4:1.

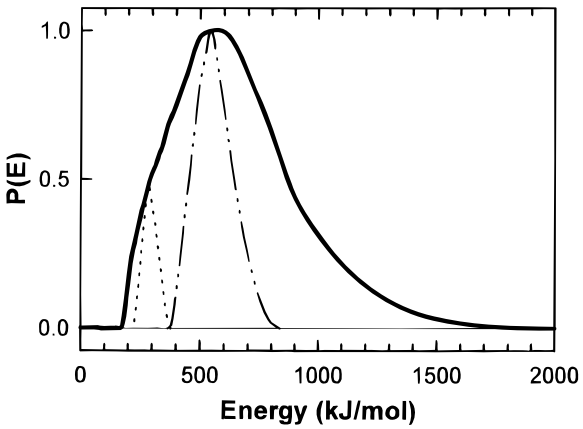

Figure 1. Translational energy distributions of the overall fluorine atom beam pulse and two portions of the pulse that were selected for the scattering experiments. The average incident energies of the two selected beam components were 284 and 544 kJ/mol.

The target surface began as epitaxial Si(100) that was cleaned ex-situ and transferred in air to the apparatus.[12] The sample mount was held at a constant temperature of 72 ± 1 °C, as indicated by a thermocouple. The absolute surface temperature was determined to be 72 °C from a beam−surface inelastic scattering experiment in which a chopped beam of near-thermal SF_6 molecules was employed. The flux-weighted angular distribution of scattered SF_6 molecules was cosine (about the surface normal), indicating that the impinging molecules had come into thermal equilibrium with the surface before desorbing with a Maxwell−Boltzmann distribution of velocities. The peak value in the measured time-of-flight distributions of scattered SF_6 molecules is thus given by $t_{max} = (d/2)(m/RT)^{1/2}$, where d is the distance from the surface to the ionizer, m is the mass of the desorbing particle, and T is the surface temperature. Before inelastic scattering data were collected for a particular combination of incident energy and angle, a steady-state condition was established where the time-of-flight distribution (at an arbitrary final angle θ_f) of the dominant reactive product (detected at SiF_3^+) no longer changed with time. Once such a condition was reached, time-of-flight distributions of scattered fluorine atoms continued to be superimposable indefinitely. Because data were collected under steady-state etching conditions, the scattering surface was no longer pure silicon, but a disordered and roughened SiF_x surface presumably similar to those known to exist during etching with fluorine in other plasma and beam environments.[9] Time-of-flight distributions of scattered fluorine atoms were collected for three incident angles (10°, 35°, and 60°) and a variety of final angles. Identical pairs of incident and final angles were used in the accumulation of data for both the lower- and higher-energy incident beams. For each incident angle and energy, TOF distributions were accumulated for 200 beam pulses at each final angle. The final angle was incremented until the entire (incident-angle-dependent) angular range was covered. Then the increment direction was reversed, and the cycle was repeated until a total of six TOF distributions had been recorded for every final angle. The six distributions for each final angle were then summed to yield a TOF

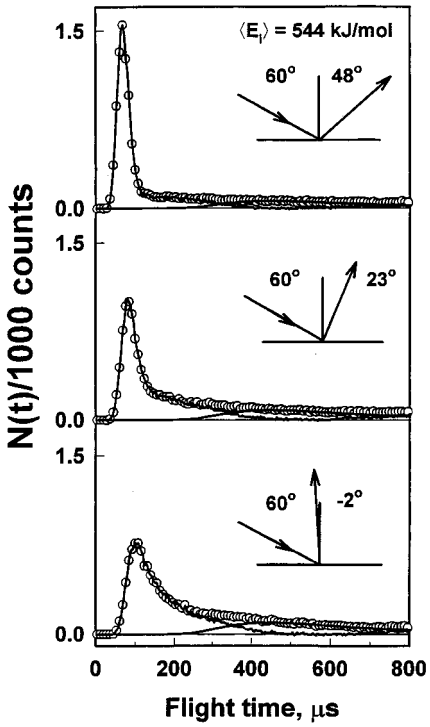

Figure 2. Representative time-of-flight distributions for fluorine atoms scattering from a fluorinated silicon surface following impact at $\langle E_i \rangle = 544$ kJ/mol and $\theta_i = 60°$. Detector (exit) angles for each distribution are given in each respective panel. Time zero is the nominal time at which the incident fluorine atom pulse strikes the surface.

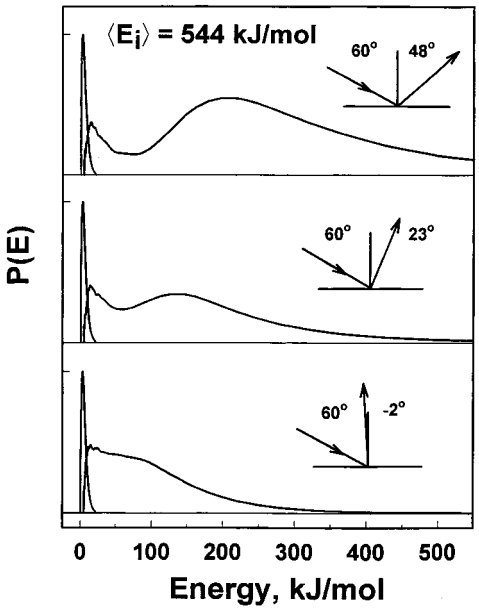

Figure 3. Translational energy distributions of scattered fluorine atoms derived from the time-of-flight distributions in Figure 2. Each distribution is divided into trapping desorption (Maxwell−Boltzmann) and inelastic scattering components.

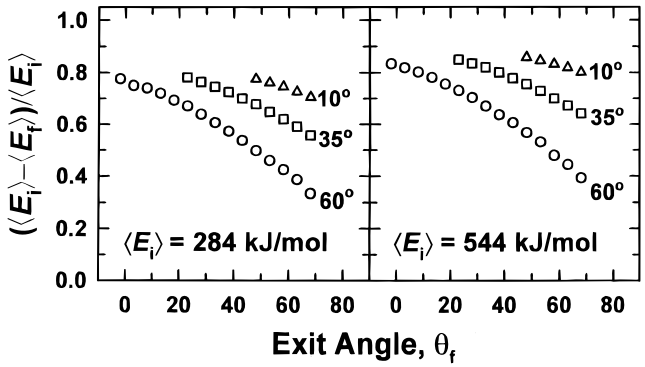

Figure 4. Average fractional energy transfer of inelastically scattered fluorine atoms as a function of exit angle for the three incident angles and two incident energies used. The final energies include contributions from all scattered fluorine atoms, regardless of the scattering mechanism.

distribution whose relative magnitude and shape were minimally affected by long-term drifts in the experimental parameters. The TOF distributions presented here have been corrected for the ion flight time from the Brink ionizer to the Daly ion counter, $2.3(m/z)^{1/2}$.

III. Results and Analysis

Figure 2 contains representative TOF distributions for fluorine atoms scattering from a silicon surface at three final angles following impact at $\langle E_i \rangle = 544$ kJ/mol and $\theta_i = 60°$. Time zero in these distributions corresponds to the time during the beam pulse at which F atoms with the average kinetic energy of the pulse strike the surface. One main peak dominates at all final angles, and this peak grows and becomes faster (shorter flight times) as the collisions become more grazing (larger final angles). A relatively small signal persists at long flight times and begins to rise slowly after about 700 μs. This slow rise is the beginning of a broad, weak signal which covers many milliseconds in arrival time. Given the slow arrival times of this broad signal and the fact that its magnitude increases with increasing pressure behind the nozzle, we attribute the slowly-rising signal at long flight times to thermalized F atoms or unprocessed SF_6 molecules which leave the nozzle at near-thermal velocities and arrive at the target long after the initial beam pulse has struck the target surface. While this persistent signal was minimized, it was not eliminated and thus contributed an uncertain amount to the signal from F atoms that exited the surface at slow velocities. Assuming all near-thermal species exited the nozzle with less than 20 kJ/mol of kinetic energy, they could not have reached the surface in less than 600 μs; thus, signal which arrived at the detector within this time should only correspond to scattered F atoms that originated in the hyperthermal beam pulse. F atoms which exit the surface at velocities given by the surface temperature would give maximum signal at a flight time of 420 μs. Although weak, signal at this flight time is clearly present, indicating that a small fraction of the incident F atoms lose essentially all their kinetic energy to the surface.

As in earlier treatments of gas−surface scattering,[13] we describe nonreactive scattering of F atoms on fluorinated silicon in terms of two basic processes, trapping desorption (TD) and inelastic scattering (IS). TD is a thermal process, while IS comprises single- and multiple-collision interactions on the surface that occur on a time scale too short for attainment of thermal equilibrium. We began deconvoluting the contributions of the two processes in a particular TOF distribution by calculating the expected TOF distribution for F atoms that would desorb from the surface in a Maxwell−Boltzmann velocity distribution at the surface temperature, and we normalized this TD component such that it matched the data at flight times in the vicinity of 500 μs. Next we subtracted the calculated TD component from the overall TOF distribution to obtain the IS component. Finally, we converted the IS component from a number density distribution as a function of time *N(t)* to a probability density function of kinetic energy *P(E)*. This analysis was done with a direct inversion procedure which assumed a monoenergetic incident beam.

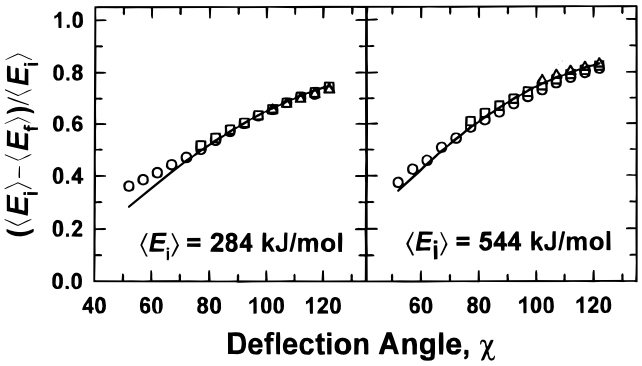

Figure 5. Average fractional energy transfer of inelastically-scattered (IS) fluorine atoms as a function of deflection angle for the three incident angles and two incident energies used. The symbols correspond to data taken at different incident angles and follow the same labeling convention as in Figure 4. The solid curves show fractional energy transfers predicted from the hard-sphere kinematic model for $\mu = 0.42$ (left panel) and $\mu = 0.52$ (right panel), where μ is the mass ratio m_F/M_s between the impinging fluorine atom and the effective surface mass.

Figure 3 shows the translational energy distributions that were derived from the TOF distributions in Figure 2. The peak of each Maxwell−Boltzmann (TD) energy distribution has been normalized to one, and the areas of each set of TD and IS distributions are proportional to the respective fluxes of F atoms that scatter by the two processes. The kinetic energy distributions for the IS component appear to be bimodal, especially for the more grazing collisions. The apparent probability of kinetic energies above the average beam energy of 544 kJ/mol reveals the limitation of the monoenergetic beam approximation; however, the determination of the average translational final translational energy was minimally affected.[14] The average energies of the F atoms which scattered at each exit angle were calculated for each of the three incident angles and then used to calculate the average fractional energy transfers shown in Figure 4. We observed that energy transfer increased when atoms either approached or exited more perpendicular to the surface. Energy transfer was least for grazing incidence trajectories with grazing exit angles. The most grazing collisions studied showed average fractional energy transfers almost down to 30%, while the least grazing collisions exhibited energy transfers in excess of 80%. Average energy transfers for F atoms increased by about 10% for a particular θ_i and θ_f when the average incident energy was almost doubled from 284 to 544 kJ/mol.

Figure 5 shows the average fractional energy transfers in the IS component (from Figure 4) plotted as a function of deflection angle, defined as $\chi = 180° - (\theta_i + \theta_f)$. In the scattering plane, the average fractional energy transfer depends not on the incident or final angle alone but on the angle through which the impinging F atom is deflected by the surface. Such a dependence has been observed in other experiments involving hyperthermal atoms scattering from solid[15] or liquid[11,16] surfaces; all these analogous results are consistent with a hard-sphere model for single atom−surface collisions.[1] The solid curves shown in Figure 5 have been generated with the hard-sphere model where optimized atom/surface mass ratios μ were found to be 0.42 and 0.52 for the lower and higher incident energy scattering conditions, respectively. The hard-sphere model equation does not take into account surface atom motion or the gas−surface attractive potential; however, these effects should be negligible for the high incident energies employed in our experiments. While the observed energy transfers are virtually identical for the same deflection angle when the incident energy is 284 kJ/mol, the strict dependence breaks down somewhat

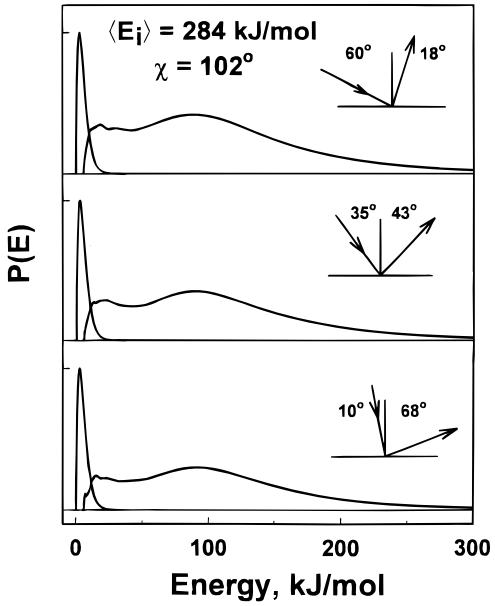

Figure 6. Translational energy distributions of scattered fluorine atoms following impact at 284 kJ/mol. The incident and exit angles corresponding to each distribution differ, but the deflection angles are all equal to 102°.

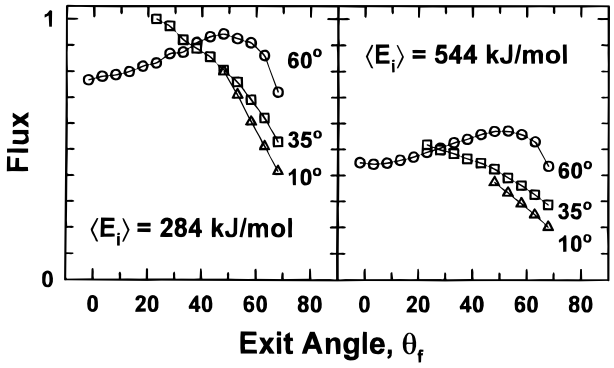

Figure 7. Flux-weighted total angular distributions of scattered fluorine atoms as a function of exit angle for the three incident angles and two incident energies used.

when the incident energy is increased to 544 kJ/mol, where we observe that larger incident angles tend to yield slightly smaller energy transfers even when the deflection angle is the same. The detailed shape of the translational energy distributions for inelastically-scattered F atoms also appears to depend mainly on the deflection angle (Figure 6).

The flux-weighted total angular distributions of scattered F atoms are plotted in Figure 7 as a function of θ_f for the two incident energies used.[17] These data have been normalized to the fluxes of the two incident beams and then renormalized with respect to the resulting maximum intensity. For both incident beams, F atoms are scattered over a wide angular range. There is more scattered flux at all angles (within the scattering plane) from the lower-energy beam than from the higher-energy beam, indicating that higher energy collisions lead to more out-of-plane scattering and/or more reaction. Our earlier modeling results suggest more reaction at higher energies.[3]

IV. Discussion

A. Energy Transfer. Rettner *et al.*[15] have pointed out that the observed scattering behavior, where the energy lost by an incident atom increases with deflection angle, is indicative of hard-sphere scattering. The dependence of average fractional energy transfer on deflection angle (Figure 5) suggests that a

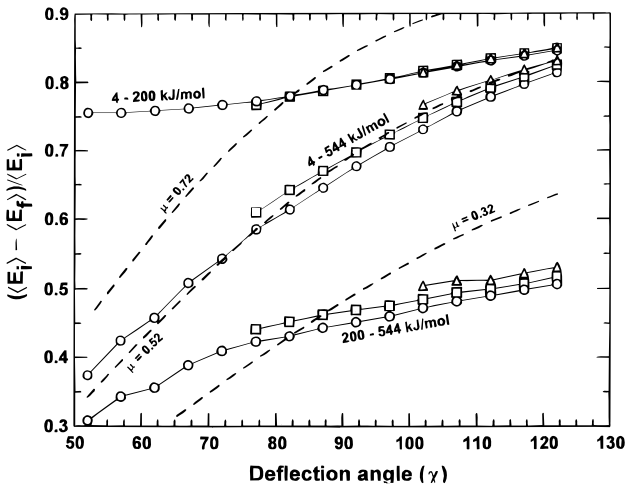

Figure 8. Average fractional energy transfers for 544 kJ/mol fluorine atoms that scatter in the IS mode into various deflection angles. Each set of curves corresponds to scattered fluorine atoms whose final energies have been averaged over the selected ranges shown. The three individual curves in each set correspond to the three incident angles used. The dashed lines show fractional energy transfers predicted from the hard-sphere kinematic model for three different mass ratios μ. Only the overall average fractional energy transfers (averaged over the entire IS final energies, 4−544 kJ/mol) apparently agree with the model prediction.

simple hard-sphere kinematic model, based on single collisions at the atom−surface interface, can describe fairly well the inelastic scattering of fast F atoms on a fluorinated silicon surface. The almost insignificant trapping desorption component in the TOF distributions also supports the picture of scattering implied by this model, as multiple inelastic collisions are required to bring an impinging atom into thermal equilibrium with the surface. On the other hand, the structure in the translational energy distributions might appear to be a manifestation of multiple scattering events at the surface. Furthermore, successful modeling of etch profile evolution[3] required the assumption of significant multiple-bounce scattering. These apparently conflicting observations reflect the intricate nature of the scattering of hyperthermal F atoms on the complex fluorinated silicon surface.

Many complex interactions are possible on this highly corrugated surface. At any given deflection angle, higher final energies may frequently come from multiple forward scattering events, whereas lower final energies are a likely result of random multiple scattering events that tend to drive the incident atom and surface toward thermal equilibrium. Between small and large deflection angles, the effective atom/surface mass ratio μ may decrease as the dominant surface collisions change from glancing blows on protruding molecular fragments to head-on impacts with these and the more sterically shielded groups at the surface. In short, the translational energy distributions of scattered F atoms reflect the combined effects of myriad possible scattering events.

Examination of the translational energy distributions reveals the fortuitous validity of the single-collision, hard-sphere-model picture of the present scattering system. Figure 8 shows plots of fractional energy transfer as a function of deflection angle. Each set of curves corresponds to F-atom final energies which have been averaged over a selected energy range. (Note that the entire range of final energies for atoms that scatter in the IS mode is considered to be 4−544 kJ/mol.) The average fractional energy transfer is seen to be a weak function of deflection angle for final energies below ∼200 kJ/mol, while energy transfers that lead to higher final energies vary significantly with deflection angle. Regardless of the energy range chosen, however, the change in average fractional energy transfer with deflection angle cannot be predicted with the hard-sphere model equation for single collisions (note examples of hard-sphere model curves predicted for different mass ratios). In addition, the energy transfer corresponding to the most probable energy in each final energy distribution (not shown) does not follow this hard-sphere model. Only the average fractional energy transfer for the entire range of final F-atom energies comes close to obeying simple hard-sphere kinematics. These observations suggest that the complex atom−surface collision dynamics behave, *on average*, like single-bounce hard-sphere scattering. Even though the hard-sphere model cannot predict the functional dependence of the fractional energy transfer for a selected energy range, the near coalescence of the three curves for each energy range indicates that the average fractional energy transfer for *any* given final energy range in the IS translational energy distribution still depends only on the deflection angle.

Figure 5 shows that the overall average fractional energy transfer depends on deflection angle only at constant incident energy. The best-fit curves from the hard-sphere model equation yield effective atom/surface mass ratios of 0.42 and 0.52 for incident F atoms with 284 and 544 kJ/mol, respectively. The different mass ratios imply a "lighter" effective surface for the higher impact energy. Two explanations are consistent with these observations. At higher impact energies, (1) collisions are faster and therefore more localized, or (2) penetration into the surface is deeper and more energy is transferred, giving the appearance of a lighter surface mass when the hard-sphere model equation is used. The incomplete coalescence of the three curves corresponding to the higher incident energy (right panel in Figure 5) may be a result of a weak dependence of the penetration depth, or effective surface mass, on incident angle at high impact energies.

The fairly constant average final energy at the low-energy range of the translational energy distributions (Figure 8) is suggestive of multiple collisions which lead to a partial loss of "memory" of the incident energy and angle. In particular, the low-energy peak in the translational energy distributions strongly suggests multiple collision events that lead to significant energy loss. A "double-backward" scattering mechanism has been proposed to explain a low-energy shoulder in the translational energy distributions observed when argon atoms scatter from liquid metals.[10] This mechanism may be ruled out here because it predicts only a few kJ/mol in translation (somewhat dependent on deflection angle), which is much less than the translational energy of the low-energy peak, approximately constant at 25 kJ/mol. A "double-forward" scattering mechanism may also be ruled out because it predicts far too much energy in translation to explain the low-energy peak. Although the explanation for the structure in the low-energy range of the translational energy distributions eludes us at this time, it must involve more complicated multiple-bounce scattering than can be represented by a simple two-bounce mechanism.

In summary, the simple hard-sphere model of scattering that assumes single atom−surface collisions can predict some of the behavior seen in these and other studies; however, its apparent successes should not be construed as validation of the assumption that the dominant scattering mode involves single collisions at the surface. Fractional energy transfer may depend on deflection angle, and under some circumstances may appear to follow the predicted angular dependence of the model, even when multiple-bounce collisions dominate the scattering dynamics.

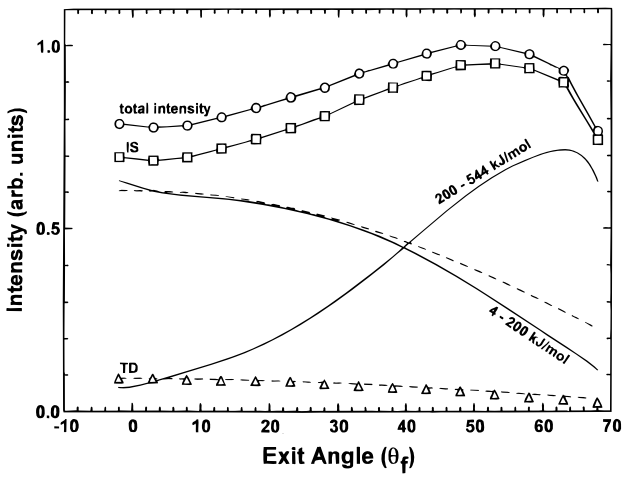

Figure 9. Flux-weighted angular distributions of scattered fluorine atoms following impingement at $\langle E_i \rangle = 544$ kJ/mol and $\theta_i = 60°$. The total angular distribution (top curve) has been separated into the inelastic scattering (IS) and trapping desorption (TD) components. The IS angular distribution has been further separated arbitrarily into two components, one corresponding to fluorine atoms with final energies less than 200 kJ/mol and the other corresponding to fluorine atoms with final energies greater than 200 kJ/mol. The dashed lines show normalized cos θ_f distributions for comparison.

B. Angular Distributions. The angular distributions of the scattered F-atom flux provide a means to describe, albeit crudely, two distinct modes of inelastic scattering. Figure 9 illustrates a deconvolution of the angular distribution following impingement of 544 kJ/mol F atoms at an incident angle of 60°. The top curve is the total scattered intensity as a function of exit angle, and the curve just below it shows the angular distribution of the entire inelastic component. The bottom curve is the distribution of the TD component, which closely follows a cosine distribution. The curves for the TD and IS components add to give the top, overall angular distribution. The two remaining curves represent an arbitrary deconvolution of the IS distribution. The curve with a maximum near the specular scattering direction shows the angular distribution of scattered F atoms with final translational energies greater than 200 kJ/mol, and the complementary curve shows the angular distribution of F atoms with final energies less than 200 kJ/mol. It is clear that in the lower energy range, where the average translational energy is approximately constant, the angular distribution falls off with exit angle, while in the higher energy range, the flux increases with a peak near the specular angle. While the selection of the 200 kJ/mol threshold for the separation of the translational energy distribution is arbitrary,[18] such a deconvolution provides evidence for two distinct kinds of scattering. The lower energy component resembles a cosine distribution (although it falls off slightly more rapidly with angle than a cosine function). If an F atom lost memory of its incident angle through multiple collisions at the surface, a cosine distribution of exit angles might be expected.[19] However, if the incident F atom underwent a single collision or multiple forward collisions at the rough surface, then we would expect an enhancement in the scattered flux in the forward direction, perhaps near the specular angle. Our observations thus suggest a first-order distinction in the nature of the nonthermal scattering at the surface. Both types of scattering involve a range of complex interactions at the surface, but one leads to loss of memory of the incident angle while the other does not. The retention of some degree of hyperthermal energy in the scattered atoms even when the angle is largely "thermalized" may be the result of a combination of factors, including the high incident energy, the highly corrugated surface, and the effective mass ratio of the collision partners at the surface.

An approximation for the deconvolution of the IS angular distribution was used in a model for etch profile evolution described earlier,[3] where the "memory-loss" scattering was shown to play an important role. For the purposes of this model, it was assumed that all F atoms with final energies less than 96 kJ/mol exited the surface in a cosine distribution about the surface normal, while atoms that retained more than 96 kJ/mol of translational energy were assumed to exit the surface in a Gaussian distribution about the specular direction. These two distributions were assumed to correspond, respectively, to multiple- and single-bounce inelastic scattering. The approximation of two simple functions for the angular distributions was essential to the success of the model, thus illustrating the significance of the memory-loss events not only to etching but as a scattering mechanism for hyperthermal F atoms on a fluorinated silicon surface.

V. Conclusion

We have observed scattering of hyperthermal fluorine atoms, with energy and angular resolution, from a complex fluorinated silicon surface during steady-state etching. Although the surface was not characterized, the scattering dynamics show remarkable structure. Two beams of fluorine atoms, with incident energies different almost by a factor of two, show similar scattering dynamics, with two key differences: (1) the effective surface mass is ~20% higher for 284 kJ/mol incident F atoms than for 544 kJ/mol incident F atoms, suggesting more surface penetration or a more localized atom−surface interaction at higher energies; (2) in the scattering plane, the flux of scattered F atoms is approximately twice as high for the lower-energy incident atoms, which may be explained by more out-of-plane scattering and/or more reaction at higher incident energies. A hard-sphere kinematic model based on single atom−surface collisions appears to work well to predict the overall average fractional energy transfer as a function of deflection angle for the inelastically-scattered atoms, but this model cannot hold rigorously because the apparent effective surface mass is energy dependent. More importantly, however, the validity of the hard-sphere model is fortuitous because (1) it does not hold for any subset of scattered F atoms, and (2) the angular distributions, the bimodal translational energy distributions, and earlier modeling studies of etching clearly indicate that *multiple*-bounce collisions dominate even the seemingly direct scattering events. Nevertheless, even when the model fails to predict the functional dependence of energy transfer, the energy transfer is still almost a constant function of deflection angle at a given incident energy. The angular distributions suggest at least two basic types of inelastic scattering, one which leads to scattered F atoms with loss of memory of the incident angle and the other which shows retention of memory of the incident angle in the direction of scattered F atoms.

Acknowledgment. This work was supported by the Ballistic Missile Defense Organization/Innovative Science and Technology Office, the Air Force Office of Scientific Research under Grant F49260-96-1-0276, and Sematech under contract No. 75017492. Support for T.A.M. came in part from a NASA fellowship. K.P.G. thanks the Camille and Henry Dreyfus Foundation for a New Faculty Award. The authors are grateful to G. M. Nathanson for many helpful discussions on the details of inelastic scattering and to G. S. Hwang for his contribution to the analysis and interpretation of the scattering data. T.K.M. expresses his gratitude to his former mentor, Prof. Y. T. Lee,

for providing the opportunity to learn chemical research in an exciting and stimulating environment and for being a source of continuing support and inspiration.

References and Notes

(1) Rettner, C. T., Ashfold, M. N. R., Eds. *Dynamics of Gas-Surface Interactions*; Royal Society of Chemistry: Cambridge, U.K., 1991.

(2) Gottscho, R. A. *Phys. World* **1993**, *6*, 39. Graves, D. B. *IEEE Trans. Plasma Sci.* **1994**, *22*, 31, and references therein.

(3) Hwang, G. S.; Anderson, C. M.; Gordon, M. J.; Moore, T. A.; Minton, T. K.; Giapis, K. P. *Phys. Rev. Lett.* **1996**, *77*, 3049.

(4) Hwang, G. S.; Giapis, K. P. *J. Vac. Sci. Technol. B* **1997**, *15*, 70.

(5) Graves, D. B.; Kushner, M. J.; Gallagher, J. W.; Garscadden, A.; Oehrlein, G. S.; Phelps, A. V. *Database Needs for Modeling and Simulation of Plasma Processing*; National Academy Press, Washington, DC, 1996.

(6) Lieberman, M. A.; Lichtenberg, A. J. *Principles of Plasma Discharges and Materials Processing*; John Wiley & Sons: New York, 1994.

(7) Pelka, J. *Microelectron. Eng.* **1991**, *14*, 269.

(8) Giapis, K. P.; Moore, T. A.; Minton, T. K. *J. Vac. Sci. Technol. A* **1995**, *13*, 959.

(9) Lo, C. W.; Shuh, D. K.; Chakarian, V.; Durbin, T. D.; Varekamp, P. R.; Yarmoff, J. A. *Phys. Rev. B* **1993**, *47*, 15648.

(10) Ronk, W. R.; Kowalski, D. V.; Manning, M.; Nathanson, G. M. *J. Chem. Phys.* **1996**, *104*, 4842.

(11) King, M. E.; Fiehrer, K. M.; Nathanson, G. M.; Minton, T. K.; *J. Phys. Chem. B* **1997**, *101*, 6556.

(12) The sample cleaning procedure involved degreasing for 10 min in boiling trichloroethylene followed by 10 min in boiling ethanol (200 proof USP), a dip in nanopure water, followed by etching for 15 s in concentrated HF (49%), a rinse in nanopure water, and finally a dip in boiling ethanol.

(13) Hurst, J. E.; Becker, C. A.; Cowin, J. P.; Janda, K. C.; Wharton, L.; Auerbach, D. J. *Phys. Rev. Lett.* **1979,** *43*, 1175. Rettner, C. T.; Schweizer, E. K.; Mullins, C. B. *J. Chem. Phys.* **1989**, *90*, 3800.

(14) For grazing collisions, energy transfer is low and final energies are high. Flight times may thus approach the temporal width of the incident beam pulse. We checked the validity of the average final energies obtained by the direct inversion method with the use of a more sophisticated forward convolution procedure. Although we are not able to correlate incident energy with final energy, we account for the incident beam distribution by assuming that it contributes to the scattered F-atom translational energy distribution $P(E_s)$ only insofar as it gives rise to a distribution of impingement times at the surface. The translational energy distribution of the incident beam $P(E_b)$ is determined from the relationship, $N(t_b) \propto P(E_b)/t_b^2$, where $N(t_b)$ is the measured TOF distribution of the incident beam pulse and t_b is the F-atom flight time from the source to the surface. The distribution of incident flux at the surface as a function of time is determined from the relationship, $P(t_b) = P(E_b)dE_b/dt_b \propto P(E_b)/t_b^3$. The goal of the analysis is the determination of the translational energy distribution of scattered F atoms $P(E_s)$. The method by which $P(E_s)$ is derived is summarized as follows: (1) guess $P(E_s)$; (2) calculate $N(t_s)$ from $P(E_s)$; (3) weight the calculated $N(t_s)$ by $P(t_b)$; (4) compare the resultant $N(t_s)$ distribution with the observed TOF distribution; and (5) repeat until a satisfactory match with the experimental TOF distribution is obtained. This method is valid when $P(E_b)$ and $P(E_s)$ are completely uncorrelated. We have found that the *average* final energy derived by this method is identical (within a few percent) to the average final energy derived from the direct inversion method for all distributions of scattered F atoms collected with the lower-energy incident beam. For the higher-energy beam, the temporal width of the incident beam pulse became significant in the determination of the average final energy when the sum of the incident and final angles was $\geq 113°$. Therefore, the average final energy derived from the forward convolution method is reported for F atoms that scatter into the four final angles, $\theta_f \geq 53°$, monitored for conditions of $\langle E_i \rangle = 544$ kJ/mol and $\theta_i = 60°$.

(15) Rettner, C. T.; Barker, J. A.; Bethune, D. S. *Phys. Rev. Lett.* **1991**, *67*, 2183.

(16) King, M. E.; Nathanson, G. M.; Hanning-Lee, M. A.; Minton, T. K. *Phys. Rev. Lett.* **1993**, *70*, 1026.

(17) The relative flux of F atoms scattered at all detected angles for all conditions was determined from the direct inversion method by integrating each derived total translational energy distribution (which is proportional to flux) from 0.2 kJ/mol to the average beam energy. We found that the calculation of relative flux as a function of final angle was insensitive to the temporal width of the incident beam pulses used in our experiments.

(18) Other energy thresholds in the range ~100−250 kJ/mol show similar qualitative behavior; however, when energy ranges that end below 200 kJ/mol are used, the angular distributions decrease with angle much faster than a cosine distribution, and when the range is extended beyond 200 kJ/mol, the angular distribution decreases slower than a cosine distribution.

(19) Preliminary calculations by one of the authors (K.P.G.) show that the cumulative flux of atoms scattered through double-, triple-, etc., bounce collisions follows closely a cosine distribution. In fact, the calculated distribution falls off slightly faster than a cosine function and resembles the 4−200 kJ/mol curve in Figure 9.